REGULAR ARTICLE

blood advances

The mitochondrial pyruvate carrier complex potentiates the efficacy of proteasome inhibitors in multiple myeloma

Steven Findlay,[1,2] Remya Nair,[3,*] Ronald A. Merrill,[4,*] Zafir Kaiser,[1,5] Alexandre Cajelot,[1,6] Zahra Aryanpour,[1] John Heath,[1,2] Catherine St-Louis,[7,8] David Papadopoli,[1,9] Ivan Topisirovic,[1,2,9,10] Julie St-Pierre,[7,8] Michael Sebag,[11] Aparna H. Kesarwala,[12] Laura Hulea,[13-15] Eric B. Taylor,[4] Mala Shanmugam,[3] and Alexandre Orthwein[1,2,9,12]

[1]Lady Davis Institute for Medical Research, Segal Cancer Centre, Jewish General Hospital, Montreal, Canada; [2]Division of Experimental Medicine, McGill University, Montreal, Canada; [3]Department of Hematology and Medical Oncology, Winship Cancer Institute, Emory University, Atlanta, GA; [4]Department of Molecular Physiology and Biophysics, University of Iowa, Iowa City, IA; [5]Department of Biochemistry, McGill University, Montreal, Canada; [6]Polytech Nice-Sophia, Université Côte d'Azur, Sophia Antipolis, Nice, France; [7]Department of Biochemistry, Microbiology, and Immunology, University of Ottawa, Ottawa, Canada; [8]Ottawa Institute of Systems Biology, Ottawa, Canada; [9]Gerald Bronfman Department of Oncology and [10]Department of Biochemistry, McGill University, Montreal, Canada; [11]The Research Institute of the McGill University Health Center, Montreal, Canada; [12]Department of Radiation Oncology, Winship Cancer Institute, Emory University, Atlanta, GA; [13]Maisonneuve-Rosemont Hospital Research Center, Montreal, Canada; and [14]Département de Biochimie et médecine moléculaire and [15]Département de Médecine, Université de Montréal, Montreal, Canada

Key Points

- Mitochondrial pyruvate import plays a critical role in regulating bioenergetic and proteolytic capacities of MM cells.

Multiple myeloma (MM) is a hematological malignancy that emerges from antibody-producing plasma B cells. Proteasome inhibitors, including the US Food and Drug Administration–approved bortezomib (BTZ) and carfilzomib (CFZ), are frequently used for the treatment of patients with MM. Nevertheless, a significant proportion of patients with MM are refractory or develop resistance to this class of inhibitors, which represents a significant challenge in the clinic. Thus, identifying factors that determine the potency of proteasome inhibitors in MM is of paramount importance to bolster their efficacy in the clinic. Using genome-wide CRISPR-based screening, we identified a subunit of the mitochondrial pyruvate carrier (MPC) complex, MPC1, as a common modulator of BTZ response in 2 distinct human MM cell lines in vitro. We noticed that CRISPR-mediated deletion or pharmacological inhibition of the MPC complex enhanced BTZ/CFZ-induced MM cell death with minimal impact on cell cycle progression. In fact, targeting the MPC complex compromised the bioenergetic capacity of MM cells, which is accompanied by reduced proteasomal activity, thereby exacerbating BTZ-induced cytotoxicity in vitro. Importantly, we observed that the RNA expression levels of several regulators of pyruvate metabolism were altered in advanced stages of MM for which they correlated with poor patient prognosis. Collectively, this study highlights the importance of the MPC complex for the survival of MM cells and their responses to proteasome inhibitors. These findings establish mitochondrial pyruvate metabolism as a potential target for the treatment of MM and an unappreciated strategy to increase the efficacy of proteasome inhibitors in the clinic.

Submitted 28 June 2022; accepted 2 March 2023; prepublished online on *Blood Advances* First Edition 15 March 2023; final version published online 13 July 2023. https://doi.org/10.1182/bloodadvances.2022008345.

*R.N. and R.A.M. are joint authors.

Data are available on request from the corresponding author, Alexandre Orthwein (alexandre.orthwein@emory.edu).

The full-text version of this article contains a data supplement.

Introduction

Multiple myeloma (MM) is the second most common hematological malignancy, accounting for ~13% of all blood cancers.[1] MM is a genetically heterogenous disease, characterized by the accumulation of malignant plasma cells in the bone marrow that display a high number of chromosomal alterations and gene mutations.[2] Patients with newly diagnosed MM who are typically treated with a proteasome inhibitor (such as bortezomib [BTZ]), an immunomodulatory drug (eg, lenalidomide), and a glucocorticoid (eg, dexamethasone) tend to respond well to this intensive therapeutic regimen[2]; however, long-term remission and cure are extremely rare, and a significant proportion of people diagnosed with MM relapse or become resistant to these drugs.[3] Nevertheless, the genetic landscape that determines the response of patients with MM to the front-line proteasome inhibitor therapies remains obscure.

Targeted and genome-wide mapping by RNA interference or CRISPR technology has identified several genetic vulnerabilities that influence the response of MM cells to proteasome inhibitors in vitro, including ribosomal function, DNA damage pathways, messenger RNA translation initiation, and proteasomal subunits.[4-8] More recently, metabolic rewiring of MM cells in response to proteasome inhibitors has emerged as an additional critical element in the development of relapsed/resistant cases.[9-14] To this end, MM cells that developed resistance to proteasome inhibitors are characterized by perturbations in cellular metabolism, including glycolysis, oxidative phosphorylation, the tricarboxylic acid (TCA) cycle, the pentose phosphate pathway, and serine synthesis.[9-11] Interestingly, BTZ-resistant MM cells appear to rely heavily on mitochondrial respiration as their principal energy source[15]; however, the factors that drive the metabolic rewiring of proteasome inhibitor resistance in MM cells remains elusive.

In this study, we performed in vitro CRISPR-based genome-wide dropout screens in 2 human MM cell lines, using BTZ as a selective agent. This approach identified the mitochondrial pyruvate carrier 1 (MPC1), a key metabolic protein that regulates the transport of pyruvate into the mitochondrial matrix, as a common modulator of BTZ response in MM cells in vitro. Genetic ablation or pharmacological inhibition of the MPC complex induces a metabolic rewiring that compromises the proteasomal activity and increases proteasome inhibitor–induced MM cell death in vitro. Importantly, several pivotal players in pyruvate metabolism exhibit altered expression in late stages of MM and correlate with poor prognosis in a cohort of patients with MM (n = 771). Together, our findings unravel the previously unrecognized importance of mitochondrial pyruvate import in MM cells and their response to proteasome inhibitors.

Methods

Cell lines and transfection

JJN3, RPMI-8226, U266B1, KMS-12BM, and 5TGM1 MM cells were cultured in RPMI-1640 medium (Wisent) supplemented with 10% fetal bovine serum (Sigma) and 1% penicillin-streptomycin (Wisent). The 5TGM1 cell line was a kind gift from Michael Tomasson (University of Iowa, IA) and Greg Mundy (Vanderbilt University, TN). All cell lines were regularly tested for mycoplasma contamination and authenticated for short tandem repeat DNA. Lentivirus was produced in HEK293T cells using calcium phosphate transfection with psPAX2 (a lentiviral packaging plasmid), VSV-g (an envelope plasmid), and 25 μM chloroquine (inhibitor of lysosomal degradation). HEK293T supernatant was collected and concentrated using 23% polyethylene glycol (50%), 8% NaCl (5 M), and 7% 1× phosphate-buffered saline (PBS). Viral infection was done in the presence of 8 μg/mL polybrene (lentiviral transduction enhancer) and 1000 μg/mL F108 to improve cellular transduction. Transduced cells were incubated at 37°C and selected 48 hours later.

CRISPR/Cas9 genome-wide screen

For the genome-wide CRISPR–CRISPR-associated protein 9 (CRISPR/Cas9)-based screen, 270 million U266/Cas9 and JJN3/Cas9 cells were transduced with TKOv1 concentrated library virus at a multiplicity of infection of 0.2, as described previously,[16] ensuring a minimum of a 600-fold coverage for each individual single guide RNA (sgRNA) represented in the cell population. Two days later, puromycin was added to the media at a final concentration of 5 μg/mL and incubated for 4 days to allow for the emergence of resistant cells with fully repaired sgRNA library–targeted loci. Cells were then split into 2 pools, each in triplicate, at a cell density of 54 million cells per replicate and treated with either vehicle (dimethyl sulfoxide [DMSO]) or BTZ at 3 nM (25% inhibitory concentration [IC_{25}]) and cultured for 2 weeks with puromycin at a concentration of 1.5 μg/mL. Cells were passaged every 3 days, maintaining a minimum cell concentration of 54 million cells per replicate to ensure that a 600-fold library coverage was maintained over the duration of selection. At each time point cell pellets were collected and frozen before genomic DNA extraction. Cell pellets were resuspended in 6 mL DNA lysis buffer (10 mM Tris–Cl, 10 mM EDTA, and 0.5% sodium dodecyl sulfate at pH 8.0) with 100 μg/mL RNase A, followed by incubation at 37°C for 60 minutes. Proteinase K was subsequently added (final concentration, 400 μg/mL), and lysates were further incubated at 55°C for 2 hours. Samples were then briefly homogenized by passing them through a 18G needle 3 times and then through a 22G needle 3 times. Sheared samples were transferred into prespun 15 mL Maxtract tubes (Qiagen) mixed with an equal volume of neutral phenol:chloroform:isoamyl alcohol (25:24:1) solution, shaken, and centrifuged at 1500*g* for 5 minutes at room temperature. The aqueous phase was extracted and precipitated with 2 volumes of ethanol and 0.2 M NaCl. Air-dried pellets were resuspended in water and quantitated via UV absorbance spectrometry.

Two-color CRISPR competitive growth assay

Next, 20 000 cells were infected at a multiplicity of infection of ~1.2 to ensure 100% transduction efficiency with either virus particles of NLS-mCherry LacZ-sgRNA or NLS-BFP GOI-sgRNA. After transduction (96 hours), mCherry- and BFP-expressing cells were mixed 1:1 and plated with or without BTZ (4 nM) in a 12-well format. The cells were subcultured when near-confluency was reached, and BTZ containing medium was replaced every 3 days. Cells were imaged for BFP and mCherry signal the day of initial plating (t = 0) and on days 4, 8, 12, and 16. Data were acquired using the fluorescence-activated cell sorter (FACS) Fortessa cytofluorimeter and processed with FACSDiva version 8.0 software (BD Biosciences).

Immunoblotting

Selected cell lines were treated as indicated before trypsinization, collection, and PBS washes. Cells were placed in 1× lithium dodecyl sulfate loading buffer (10 mM Tris-HCL, 140 mM Tris-base, 0.5 mM EDTA, 1% lithium dodecyl sulfate, and 10% glycerol) with 1× protease (Roche) and phosphatase (Sigma) inhibitors. Following sonication, cell lysates were cleared via centrifugation at maximum speed for 15 minutes at 4°C. After the addition of loading dye and 2-mercaptoethanol, cleared lysate was placed at 70°C for 10 minutes. Protein lysates were subjected to immunoblotting as previously described (Findlay et al[16]). Membranes were blocked with 5% bovine serum albumin in Tween 20 (0.015%)–tris-buffered saline for 3 hours at 4°C and probed overnight with primary antibody at a dilution of 1:1000 in Tween tris-buffered saline. Secondary antibodies were used at a dilution 1:10 000 in Tween tris-buffered saline. Signal was detected using Immobilon Western Chemiluminescent HRP substrate (GE Healthcare) and an Azure 400 machine (Azure Biosystems).

Proliferation assay

Cells were incubated with various drugs and/or with media for the times indicated in the figure legends. Cells were trypsinized and resuspended in media, and live cells were quantified via Trypan blue exclusion using a hemocytometer, daily for 4 days.

Apoptosis and cell cycle

Apoptosis was measured via flow cytometry, with annexin V-647 and propidium iodide (PI) staining. Briefly, the cells were washed twice in wash buffer (0.01 M Hepes, 0.14 M NaCl, and 2.5 mM $CaCl_2$) and stained with annexin-V-647 for 15 minutes at room temperature, followed by a final wash and the addition of 2 μg/μL of PI. Viability of cells was assessed by gating PI^+ vs PI^- cells.

Cell cycle was measured flow-cytometrically using PI. Briefly, cells were washed in PBS and fixed in 70% ethanol at 4°C overnight. The following day the cells were washed thrice with PBS and incubated with PI (1:2000). Data were acquired using FACSCanto II cytofluorimeter and processed with FACSDiva 8.0 software (BD Biosciences).

Drug preparation and treatment

BTZ, Carfilzomib (CFZ), UK-5099, CB-839 (Selleck Chemicals), and MitoTEMPO (Sigma) powder were dissolved in DMSO, filter sterilized, and stored at −20°C. For in vitro experiments, BTZ and CFZ were used at a final concentration of 2.5 to 5 nM, UK-5099 was used at a final concentration of 10 μM, CB-839 was used at a final concentration of 5 μM, and MitoTEMPO was used at a final concentration of 20 μM.

LC-MS metabolomic analysis

All liquid chromatography–mass spectrometry (LC-MS) grade solvents and salts were purchased from Fisher (Ottawa, ON, Canada: water, acetonitrile, methanol, formic acid, ammonium acetate, and ammonium formate. The authentic metabolite standards and N-ethylmaleimide were purchased from Sigma-Aldrich Co [Oakville, ON, Canada]).

Nucleotide detection and analysis was performed using LC–tandem MS (LC-MS/MS) at the Metabolomics Core Facility of the Goodman Cancer Research Centre. Cultured cells were treated with BTZ and UK-5099 for 16 and 24 hours, respectively. Cells were washed in ammonium formate 3 times, then quenched in cold 50% methanol (v/v) with acetonitrile and N-ethylmaleimide supplementation at 1 mg/mL. Cells were lysed and homogenized by bead beating for 30 seconds at 50 Hz, using 4 ceramic beads (2 mm) per sample (SpeedMill Plus, Analytik Jena). Cellular extracts were partitioned into aqueous and organic layers after dimethyl chloride treatment and centrifugation. The aqueous supernatants were dried via vacuum centrifugation, with the sample temperature maintained at −4°C (Labconco, Kansas City, MO). Dried extracts were subsequently resuspended in 50 μL of chilled H_2O and clarified via centrifugation at 1°C. Sample injection volumes for analyses were 5 μL per injection.

For targeted metabolite analysis, samples were injected onto an Agilent 6470 triple-quadrupole LC-MS/MS (Agilent Technologies). Chromatographic separation of metabolites was achieved by using a 1290 Infinity ultra-performance quaternary pump liquid chromatography system (Agilent Technologies). The mass spectrometer was equipped with a Jet Stream electrospray ionization source, and samples were analyzed in negative mode. The source-gas temperature and flow rate were set at 150°C and 13 L/min, respectively; the nebulizer pressure was set at 45 psi, and capillary voltage was set at 2000 V. Multiple reaction monitoring parameters (qualifier/quantifier ions and retention times) were either obtained or optimized using authentic metabolite standards.

Chromatographic separation of the isomers and other metabolites was achieved by using a Zorbax Extend C18 column 1.8 μm, 2.1 × 150 mm^2 with guard column 1.8 μm, and 2.1 × 5 mm^2 (Agilent Technologies). The chromatographic gradient started at 100% mobile phase A (97% water, 3% methanol, 10 mM tributylamine, 15 mM acetic acid, and 5 μM medronic acid) for 2.5 minutes, followed with a 5-minute gradient to 20% mobile phase C (methanol, 10 mM tributylamine, 15 mM acetic acid, and 5 μM medronic acid), a 5.5-minute gradient to 45% phase C, and a 7-minute gradient to 99% phase C at a flow rate of 0.25 mL/min. This was followed by a 4-minute hold time at 100% mobile phase C. The column was restored by reverse flow with 99% mobile phase D (90% acetonitrile) for 3 minutes at 0.25 mL/min, followed by increase of the flow rate to 0.8 mL/min over 0.5 minutes and a 3.85-min hold, after which the flow rate was decreased to 0.6 mL/min over 0.15 minutes. The column was then reequilibrated at 100% phase A over 0.75 minutes, during which the flow rate was decreased to 0.4 mL/min and held for 7.65 minutes. One minute before the next injection, the flow was brought back to forward flow at 0.25 mL/min. For all LC-MS analyses, 5 μL of sample was injected. The column temperature was maintained at 35°C.

Universally labeled ^{13}C-L-Glutamine tracing and LC-MS analysis

Four million U266 cells were incubated with 2 mM L-[U^{13}C]-Glutamine (Cambridge Isotope Laboratories) and the indicated drugs for 1 hour. Cells were subsequently washed with cold PBS twice and once in cold H_2O before being frozen and lyophilized without thawing and extracted using ice-cold acetonitrile:methanol:water (2:2:1) solution containing 1 μL/mL of an internal standard mix. Cell pellets were sonicated for 10 minutes,

rotated for 60 minutes at −20°C, and centrifuged at 21 000*g* for 10 minutes. The supernatant was transferred to a new 1.7-mL microcentrifuge tube and pulse vortexed, and 300 µL was transferred to a new 1.7-mL microcentrifuge tube for drying in a Speedvac Vacuum concentrator (Thermo Fisher) for 2 hours without heating at a vacuum ramp of 4. Dried metabolite extracts were resuspended in 30 µL of acetonitrile:water (1:1), vortexed for 10 minutes, and stored at −20°C overnight. The ensuing day, samples were centrifuged at 21 000*g* for 10 min, and the supernatants were transferred to autosampler vials. A quality control (QC) sample was prepared by pooling equal volumes from each sample and was processed as the other samples.

For LC-MS, 2 µL of sample was injected using a Thermo Vanquish Flex UHPLC into a Millipore SeQuant ZIC-pHILIC (2.1 × 150 mm; 5 µm particle size, Millipore Sigma #150460) column with an attached ZIC-pHILIC guard column (20 × 2.1 mm, Millipore Sigma #150437). The mobile phase was run at a flow rate of 0.150 mL/min, containing buffer A [20 mM $(NH_4)_2CO_3$ and 0.1% NH_4OH (v/v)] and buffer B (acetonitrile) with the following linear gradients: from 0 to 20 minutes buffer A from 20% to 80%, from 20 to 20.5 minutes buffer A from 80% to 20%, and from 20.5 to 28 minutes held at 20% buffer A. Data were attained using a Thermo Q Exactive MS operated in negative mode with a spray voltage set to 3.0 kV, the heated capillary held at 275°C, and the heated electrospray ionization probe held at 350°C. The sheath gas flow rate was set to 40 units, the auxiliary gas flow rate to 15 units, and the sweep gas flow rate to 1 unit. MS data resolution was set at 70 000, the automatic gain control target at 10e6, and the maximum injection time at 200 milliseconds. The QC sample was analyzed at the beginning and at the end of the LC-MS run as well as at approximately every seventh injection throughout.

LC-MS data were processed using the Thermo Scientific TraceFinder version 5.1 software. Targeted metabolites were identified based on the University of Iowa Metabolomics Core facility standard-confirmed in-house library, defining a target ion and at least 1 confirming ion and accurate mass, retention time, and MS/MS fragmentation pattern, when present. The NOREVA tool used the QC sample analyzed throughout the instrument run to apply local polynomial fits to metabolite peak areas and correct for instrument drift.[17] For ^{13}C-tracing analysis, ^{12}C–natural abundance was corrected using previously defined equations.[18]

Seahorse XF96 respirometry assay

The oxygen consumption rate and extracellular acidification rate (ECAR) were measured using a Mito Stress Test Kit and XF96 Extracellular Flux Analyzer (Seahorse Bioscience) per the manufacturer's protocol. In brief, 96-well plates were coated with CellTak at a concentration of 22.5 µg/µL, per the manufacturer's protocol, and left at 4°C overnight. On the day of measurement, cells were washed with XF base media supplemented with 10 mM glucose, 2 mM glutamine, and 1 mM sodium pyruvate (Wisent) and incubated for 1 hour to equilibrate before reading. ECAR and oxygen consumption rate measurements were taken before and after the addition of oligomycin (1 µM), carbonyl cyanide-p-trifluoromethoxyphenylhydrazone (0.25 µM), and rotenone/antimycin (1 µM) and used to calculate adenosine triphosphate (ATP) production, bioenergetic capacity, and supply flexibility index, as previously described.[19]

Metabolic assays

Lactate and glucose concentrations were measured as previously described.[20] Briefly, 100 000 cells were plated and grown in 6-well plates (35 mm) and incubated with fresh growth medium in the presence or absence of BTZ and/or UK5099 for 48 hours before sample collection. Analysis of glucose consumption and lactate production was performed on samples of the extracted media using the Nova BioProfile Analyzer 400 (Nova Biomedical) and normalized to cell number.

Proteasome activity

Cells (100 000) were plated in a 96-well plate and cultured for 24 hours before collection. Proteasomal-mediated degradation was evaluated using a 20S proteasome assay kit from Cayman Chemical per the manufacturer's protocol and normalized to cell count.

Patient data set analysis

The IA18 Release of CoMMpass data were downloaded from the MM research foundation (MMRF) researcher gateway portal, which consists of 903 RNA sequencing data sets of baseline $CD138^+$ plasma cell bone marrow samples from patients with newly diagnosed MM. Among them, overall survival or progression-free survival information was available for 771 patients, which were included in our analysis. We incorporated all patient data available, irrespective of their treatment regimen. Genes involved in pyruvate metabolism were incorporated into a multivariate Cox regression analysis (R-Studio) to generate a pyruvate metabolism gene signature. The gene signature and patient survival data were organized via quartiles with the high pyruvate signature and low pyruvate signature plotted via Kaplan Meier (Prism).

Data from 2 other RNA sequencing studies that evaluated expression throughout MM development were retrieved from the Gene Expression Omnibus database. Data of bone marrow–derived $CD138^+$ plasma cells from 7 patients with monoclonal gammopathy of undetermined significance (MGUS), 39 patients with MM, and 6 patients with plasma cell leukemia were obtained from GSE2113. Data of bone marrow–derived $CD138^+$ plasma cells from 15 healthy donors, 22 patients with MGUS, 17 patients with smoldering MM, 69 patients with MM, and 32 patients with relapsed MM were obtained from GSE6477. Expression was plotted based on the disease state.

Purification and analysis of primary MM cells

All samples used in this study were collected following an Emory University Institutional Review Board–approved protocol in compliance with all relevant ethical regulations (IRB00057236), as described previously.[21] Patient samples were stained with anti–CD38-phyocerythrin and anti–CD45-allophycocyanin-Cy7 (BD Biosciences) to identify MM cells, and cell viability was monitored via annexin-V–fluorescein isothiocyanate (BD Pharminogen) flow cytometry analysis after treatment with the indicated concentration of drug, as previously described.[22]

Statistical analyses

All quantitative experiments are plotted as graphs with the mean ± standard error of the mean, with data from the independent number of experiments indicated in the figure legend. All data sets were

tested for normal distribution by Shapiro-Wilk test. Statistical significance was determined using the test indicated in the figure legends. All statistical analyses were performed using Prism version 9 (Graphpad Software).

Results

CRISPR screening identifies MPC1 as a modulator of BTZ response in MM cells

To identify the factors that modulate BTZ response in MM cells, we used 2 different human MM lines that recapitulate some of the cytogenetic heterogeneity observed in patients with MM[2]: the U266 cell line is characterized by deletions in chromosome 13 and 17p, involving *RB1* and *TP53* genes respectively;[23] whereas the JJN3 cell line harbors an amplification of chromosome arm 1q21, a frequent chromosomal aberration in MM.[24] To ensure high genome editing capacity, we stably expressed Cas9 in both cell lines by lentiviral transduction (supplemental Figure 1A), and genome editing efficiency was confirmed by targeting FAM83G (supplemental Figure 1B).

Next, we performed CRISPR-based genome-wide screening in both human MM cell lines by transducing them with the TKO version 1 sgRNA library,[25] and selecting them with puromycin (Figure 1A). Both U266 and JJN3 transduced cell lines were subsequently treated with either BTZ IC_{25} or with vehicle (DMSO) for 21 days before being processed for next-generation sequencing analysis. MaGECK algorithm was used to determine the relative abundance of a given sgRNA and identify genes whose knockout confers either resistance or sensitivity to BTZ ($-0.2 < \beta$-score < 0.2; supplemental Table 1).[26] In both cell lines, gene set enrichment analysis identified the proteasome core complex as significantly enriched in the sensitizing arm of both screens (supplemental Figure 1C; supplemental Table 2). In fact, several subunits of the 20S proteasome (*PSMB1, PSMB4-6,* and *PSMB8)* sensitize to BTZ in both MM cell lines (Figure 1B; supplemental Figure 1D; supplemental Table 1), as previously shown.[7,8] Similarly, pathway enrichment analysis identified several processes that have been described to modulate the response to proteasome inhibitors (supplemental Figure 1C; supplemental Table 2),[8] including homologous recombination,[27-29] cell cycle,[30] and RNA-mediated processes.[8,31,32] Collectively, these findings confirmed the validity of our CRISPR-based screening approach.

Taking into consideration the high heterogeneity of MM, we focused our attention on hits that increased sensitivity to BTZ in both U266 and JJN3 cell lines ($\beta > -0.2$; Figure 1C; supplemental Table 3). This analysis revealed 75 overlapping genes that scored highly in both screens, including the transcriptional factor *IRF4* (U266: $\beta = -0.42358$; JJN3: $\beta = -0.3689$; Figure 1D), which has previously been implicated in the response to BTZ.[33] To infer clinical relevance in our analysis, we examined their RNA expression using the MMRF CoMMpass database ($n = 921$).[34] Interestingly, *MPC1*, which encodes for a subunit of the MPC complex, scored as a top gene (Figure 1E). Of note, this complex was identified a decade ago[35,36] but remains to be characterized in MM cells. In fact, our CRISPR-based approach identified several factors involved in pyruvate metabolism in at least 1 MM cell line (supplemental Figure 1C-D), including the other subunit of the MPC complex, *MPC2* (U266: $\beta = -0.14864$) as well as the pyruvate dehydrogenase complex composed of *PDHA* (U266: $\beta = -0.16121$) and *PDHB* (U266: $\beta = -0.19437$; JJN3: $\beta = -0.13871$). These data suggest that pyruvate metabolism may play an important role in the response of MM cells to BTZ in vitro. Thus, we focused our attention on the role of mitochondrial pyruvate import and validated this hit using a CRISPR-based 2-color competition assay (Figure 1F).[37] We targeted *MPC1* with 3 unique sgRNAs (sgMPC1-1, -2, and -3) coupled to blue fluorescent protein (BFP) in U266 cells and used a sgRNA targeting LacZ (sgCtrl) coupled to mCherry as control. Although targeting *MPC1* only modestly affected cell proliferation at steady state (DMSO, ~25%; Figure 1G), it strongly sensitized U266 cells to BTZ (3 nM) in this assay (~55%). Altogether, these data point toward an important contribution of MPC1 in the response of MM cells to BTZ in vitro.

Targeting the MPC complex exacerbates BTZ-induced MM cell death

MPC is a 150 kDa complex composed of both MPC1 and MPC2, which transports pyruvate across the inner mitochondrial membrane.[38] To better understand how the MPC complex influences BTZ response in MM cells in vitro, we generated *MPC1* knockout clones (sgMPC1-1 and -2) in both JJN3 and U266 cells using CRISPR technology (supplemental Figure 1D-E). Interestingly, loss of MPC1 correlated with a drastic reduction in endogenous MPC2 protein levels (supplemental Figure 1E), highlighting the interdependent relationship between both MPC subunits.[39] Firstly, we monitored the proliferative capacity of these clones and their respective cycle distribution, and we confirmed that *MPC1* deletion has limited impact on untreated MM cells (supplemental Figure 1G-I). Still, MPC1-depleted JJN3 cells displayed higher sensitivity to BTZ ($IC_{50} = 5.3\text{-}5.6$ nM) compared with control cells ($IC_{50} = 6.6$ nM; supplemental Figure 1J).

We further investigated the contribution of MPC1 in the modulation of BTZ response by monitoring clonal viability through PI staining in the presence of BTZ (4 nM, 48 hours) or vehicle control. As expected, MPC1-deficient JJN3 and U266 clones displayed significantly higher levels of PI^+ cells upon exposure to BTZ (Figure 2A). Coupling our PI analysis with annexin-V staining, we observed a significant increase in the proportion on *MPC1*-knockout cells in late apoptosis upon BTZ treatment (Figure 2B-C). We made a similar observation using the second-generation proteasome inhibitor CFZ (4 nM, 48 hours; Figure 2D), highlighting that MPC1 abrogation potentiates the effect of proteasome inhibitors in MM cells.

The MPC complex can be targeted by a series of inhibitors,[40] including the cell permeable α-cyanocinnamate compound UK-5099, which specifically modifies a thiol group of a cysteine on the carrier (Figure 2E). We took advantage of this drug to further characterize the link between the MPC complex and the response to proteasome inhibitors in MM cells. In this set of experiments, we tested a panel of both human (JJN3, U266, RPMI-8266, and KMS-12-BM) and mouse (5TMG1) MM cell lines that have different intrinsic sensitivities to BTZ (supplemental Figure 2A) and exposed them to a suboptimal dose of BTZ that, when applied alone, had limited effect on cell viability as monitored by PI staining (Figure 2F). Of note, UK-5099 treatment alone did not cause any significant increase in the proportion of PI^+ cells in the MM cell

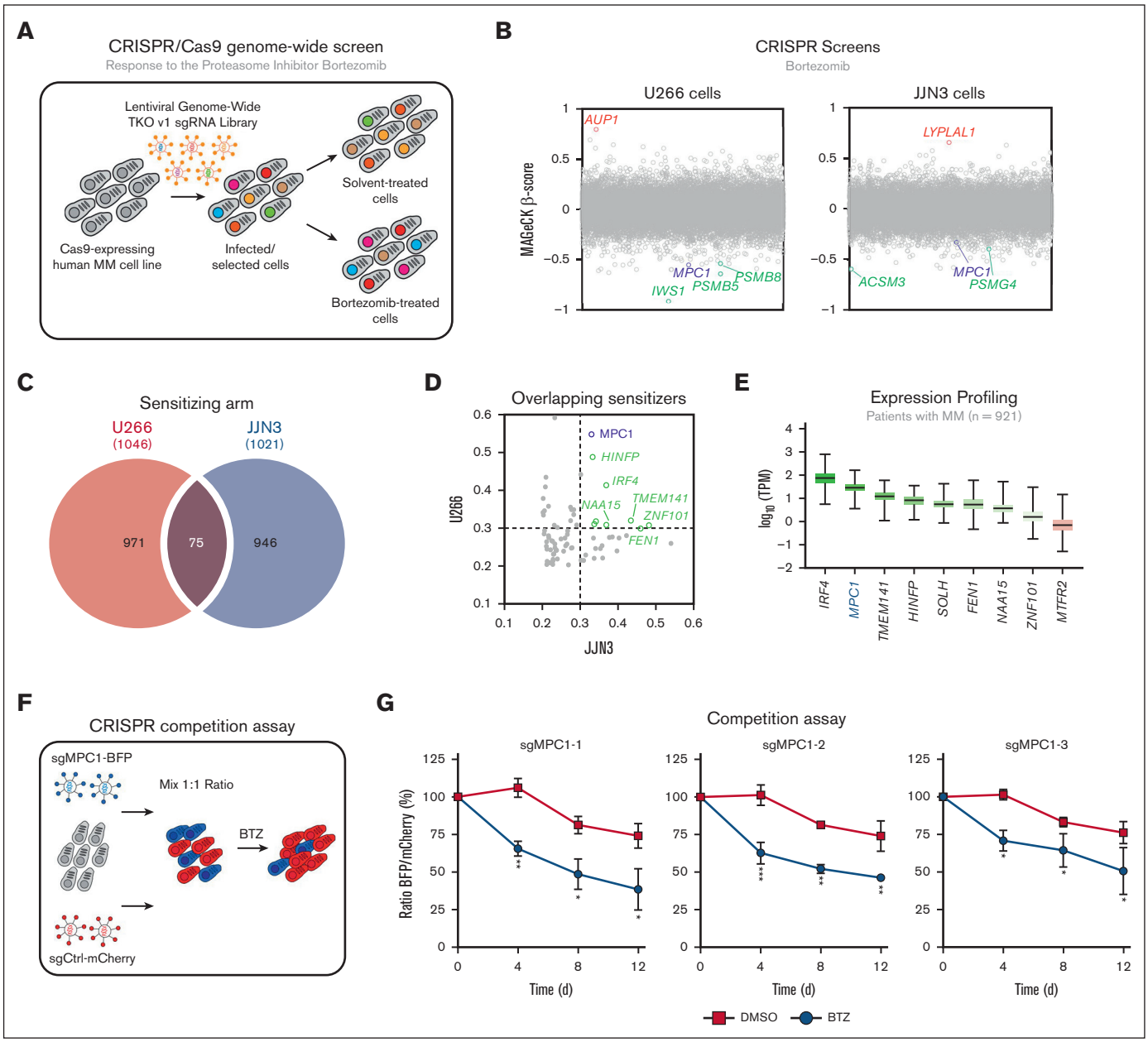

Figure 1. CRISPR screening identifies MPC1 as a modulator of BTZ response in MM cells. (A) Schematic of our CRISPR-based genome-wide screening pipeline developed in MM cells. (B) Representation of the CRISPR-based dropout screen performed in U266 and JJN3 cells in the presence of BTZ (IC_{25}). Genes are represented in alphabetically order with their respective MAGeCK β-score. (C) Overlapping genes from U266 and JJN3 sensitizing arms (MAGeCK $\beta \leq -0.2$). (D) Representation of the overlapping sensitizers identified in panel C with their respective MAGeCK β-score in JJN3 cell line (x-axis) and U266 cell line (y-axis). (E) Expression analysis of the 75 overlapping sensitizers in the MMRF CoMMpass database (n = 921). The top 9 most-expressed genes are represented in this panel. (F) Competitive growth assay in the presence or absence of BTZ (3 nM) or DMSO (vehicle) in U266 cells. Data are represented as the ratio of BFP:mCherry$^+$ ± standard error of the mean, normalized to day 0 (3 different sgRNAs; n = 3). Significance was determined using two-way ANOVA followed by a Sidak test. *$P \leq .05$; **$P \leq .01$; ***$P \leq .005$. ANOVA, analysis of variance; BFP, blue fluorescent protein.

lines tested (Figure 2F). However, UK-5099 potentiated the effect of BTZ, because of which their combination significantly reduced MM cell viability in vitro (Figure 2F). Importantly, combining UK-5099 with BTZ rapidly affected MM cell viability, peaking at 48 hours after treatment relative to each inhibitor alone (supplemental Figure 2B). Another surrogate method to monitor cell death relies on the presence of cells with fractional DNA content, designated as the sub-G1 population.[41] The analysis of our cell cycle data revealed a more dramatic induction of a sub-G1 population upon treatment with both BTZ and UK-5099 as compared with each single treatment (supplemental Figure 2C). Consistent with these data, annexin-V/PI staining showed a significant increase in the proportion of early and/or late apoptotic cells upon exposure to both UK-5099 and a proteasome inhibitor (BTZ or CFZ) relative to

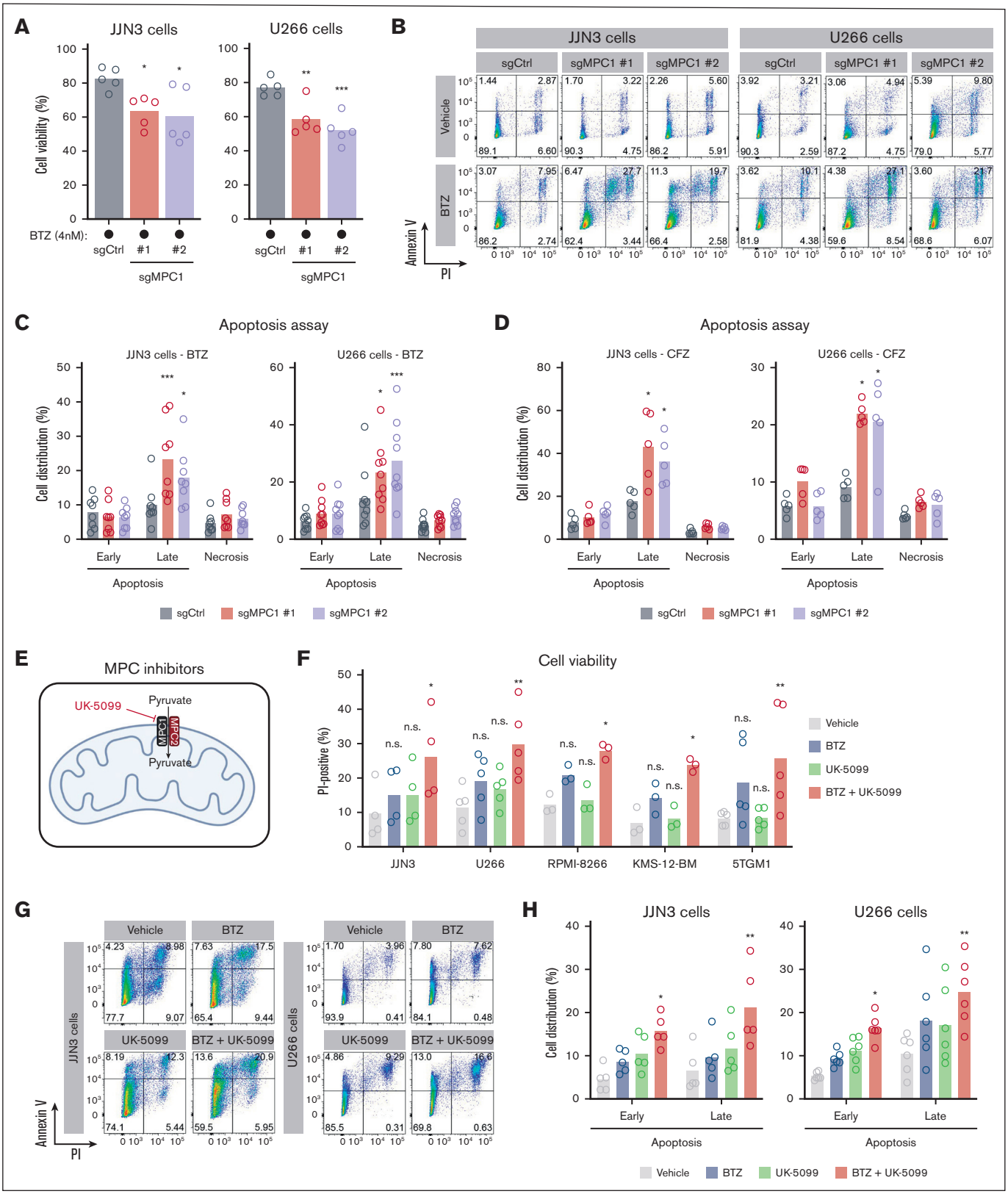

Figure 2. Targeting the MPC complex exacerbates BTZ-induced apoptosis of MM cells. (A) JJN3 and U266 cells were treated with BTZ (4 nM) for 48 hours, followed by an assessment of cell viability via PI staining (n = 5). Significance was determined using one-way ANOVA followed by a Dunnett test. *$P \leq .05$; **$P \leq .005$; ***$P \leq .005$. (B) Representative flow cytometry analysis of JJN3 and U266 cells treated with either DMSO or BTZ (4 nM) for 48 hours and stained with annexin-V/PI. (C) Representation of the

vehicle controls (Figure 2G-H; supplemental Figure 2D-E). Altogether, these data suggest that genetic or pharmacological targeting of the MPC complex enhances proteasome inhibitor–induced cell death in MM cells in vitro.

The MPC complex determines the bioenergetic capacity of MM cells under stress

The MPC complex plays a pivotal role in cell metabolism by promoting the transport of pyruvate derived from glycolysis, providing a major substrate for mitochondrial respiration, thereby fueling the TCA cycle and boosting oxidative phosphorylation.[42] To better understand the role of the MPC complex in MM cells, we analyzed the bioenergetic profiles of both JJN3 and U266 MM cell lines, using the Seahorse bioanalyzer. Abrogation of MPC1 resulted in a decrease in both basal and maximal respiration rates as well as a reduced spare respiratory capacity as compared with MPC1-proficient JJN3 and U266 controls (Figure 3A-B). In turn, ECAR measurement under mitochondrial stress showed a significant increase under basal conditions between *MPC1*-knockout and control clones (Figure 3C; supplemental Figure 3A). These data correlated with a rapid depletion of glucose and a significant enrichment of lactate in the media of MPC1-deficient vs -proficient JJN3 and U266 cells (Figure 3D; supplemental Figure 3B), suggesting that abrogation of MPC1 results in increased glycolysis as a compensatory mechanism for the respiratory defects that we observed (Figure 3A-B). Next, we quantified the effect of targeting MPC1 on maximal theoretical ATP production from oxidative phosphorylation [JATP(Ox)] and glycolysis [JATP(Glyc)].[19] Consistent with these experiments, we noticed that MPC1 abrogation decreased JATP(Ox) (Figure 3E-F). Albeit a concomitant increase in JATP(Glyc), MPC1 loss strongly impaired total cellular bioenergetic capacity [JATP(Ox) + JATP(Glyc)] in both JJN3 and U266 cell lines (Figure 3E-F). Altogether, these data indicate that MPC1 plays a key role in the bioenergetic capacity of MM cells in vitro.

Targeting the MPC complex alters glutamine metabolism in MM cells

To better understand how mitochondrial pyruvate import enhances the response of MM cells to BTZ, we extended our metabolic analysis to the pharmacological inhibition of both pathways. Consistent with our genetic study, inhibiting the MPC complex with UK-5099 significantly impaired both basal and maximal respiration of U266 cells (Figure 4A), which was accompanied by an increased glucose uptake and lactate secretion in the media (supplemental Figure 4A), a phenomenon that was also observed in combination therapy with both UK-5099 and BTZ. In turn, BTZ only minimally affected basal respiration and maximal respiration capacity of U266 cells (Figure 4A), with no significant changes in the levels of either glucose or lactate in the media as compared with vehicle-treated controls (supplemental Figure 4A).

To further investigate whether metabolic perturbations could explain how MPC1 loss potentiates the cytotoxic effect of proteasome inhibitors, we performed a systematic LC-MS–based metabolomic profiling. As expected, we observed a significant accumulation of intracellular pyruvate in U266 cells treated with UK-5099 in the presence or absence of BTZ, with a concomitant decrease in TCA cycle intermediates, such as citric acid/isocitrate, cis-aconitic acid, and α-ketoglutarate (α-KG; Figure 4B-C; supplemental Figure 4B). We extended our metabolomic profiling to JJN3 cells and observed similar metabolic perturbations upon treatment with UK-5099 in the presence or absence of BTZ (supplemental Figure 4C). As previously observed in U266 cells, inhibiting the MPC complex with UK-5099 was accompanied by an increased glucose uptake and lactate secretion in the media in JJN3 cells (supplemental Figure 4A).

High glycolytic flux has been associated with increased reactive oxygen species, which can promote cell death.[43,44] Therefore, we wondered whether the metabolic perturbations observed in MM cells upon treatment with UK-5099 could result in the production of reactive oxygen species, thereby potentiating proteasome inhibitor–induced cell death in vitro. We took advantage of the mitochondria-targeted antioxidant MitoTEMPO that has been described for its effective superoxide scavenging properties.[45] Interestingly, cotreatment of U266 cells with MitoTEMPO did not abolish the effect of UK-5099 in enhancing BTZ-induced MM cell death (supplemental Figure 4D). In fact, pyruvate supplementation, which has previously been shown to have antioxidative properties,[46] promoted MM cell death, even in the absence of BTZ (supplemental Figure 4E). These data suggest that more complex mechanisms may be at play in targeting of the MPC complex to potentiate BTZ-induced MM cell death.

Inhibition of the MPC complex and subsequent reduction in mitochondrial pyruvate import is known to induce glutamine anaplerosis, resulting in metabolite entry into the TCA cycle.[47] Inversely, proteasome inhibition has been shown to downregulate glutaminases,[48] thereby suggesting that combinatorial targeting may simultaneously reduce mitochondrial pyruvate import and glutaminolysis. We therefore explored the impact of combining UK-5099 with BTZ on glutamine intermediates by LC-MS. Strikingly, inhibiting both the MPC complex and the proteasome resulted in a significant alteration of glutamine metabolism marked by a depletion of glutamine in both JJN3 and U266 cells, with a concomitant increase in aspartate, a glutamine-derived amino acid (Figure 4D; supplemental Figure 4F). N-ethylmaleimide–glutathione depletion was also observed in U266 cells upon inhibition of both the MPC complex and the proteasome (Figure 4D).

Figure 2 (continued) annexin-V/PI analysis displayed in panel B for both JJN3 (n = 8) and U266 cells (n = 9). Significance was determined using two-way ANOVA followed by a Dunnett test. *$P \leq .05$; ***$P < .0001$. (D) Similar to panel C, except that BTZ was replaced by CFZ (4 nM) for both JJN3 (n = 5) and U266 cells (n = 5). Significance was determined using two-way ANOVA followed by a Dunnett test. *$P \leq .0005$. (E) Schematic representing UK-5099 inhibiting pyruvate entry into the mitochondrial matrix via MPC1 and MPC2. (F) JJN3 (n = 4), U266 (n = 5), RPMI-8266 (n = 3), KMS-12-BM (n = 3), and 5TGM1 cells (n = 5) were treated with BTZ (3 nM) and UK-5099 (10 μM) for 48 hours, followed by an assessment of cell viability via PI. Significance was determined using two-way ANOVA followed by a Dunnett test. *$P \leq .05$; **$P \leq .005$. (G) Representative flow cytometry analysis of JJN3 and U266 cells treated with either BTZ (3 nM) and UK-5099 (10 μM) for 48 hours and stained with annexin-V/PI. (H) Representation of the annexin-V/PI analysis displayed in panel G for both JJN3 (n = 5) and U266 cells (n = 6). Significance was determined using two-way ANOVA followed by a Dunnett test. *$P \leq .05$; **$P \leq .005$.

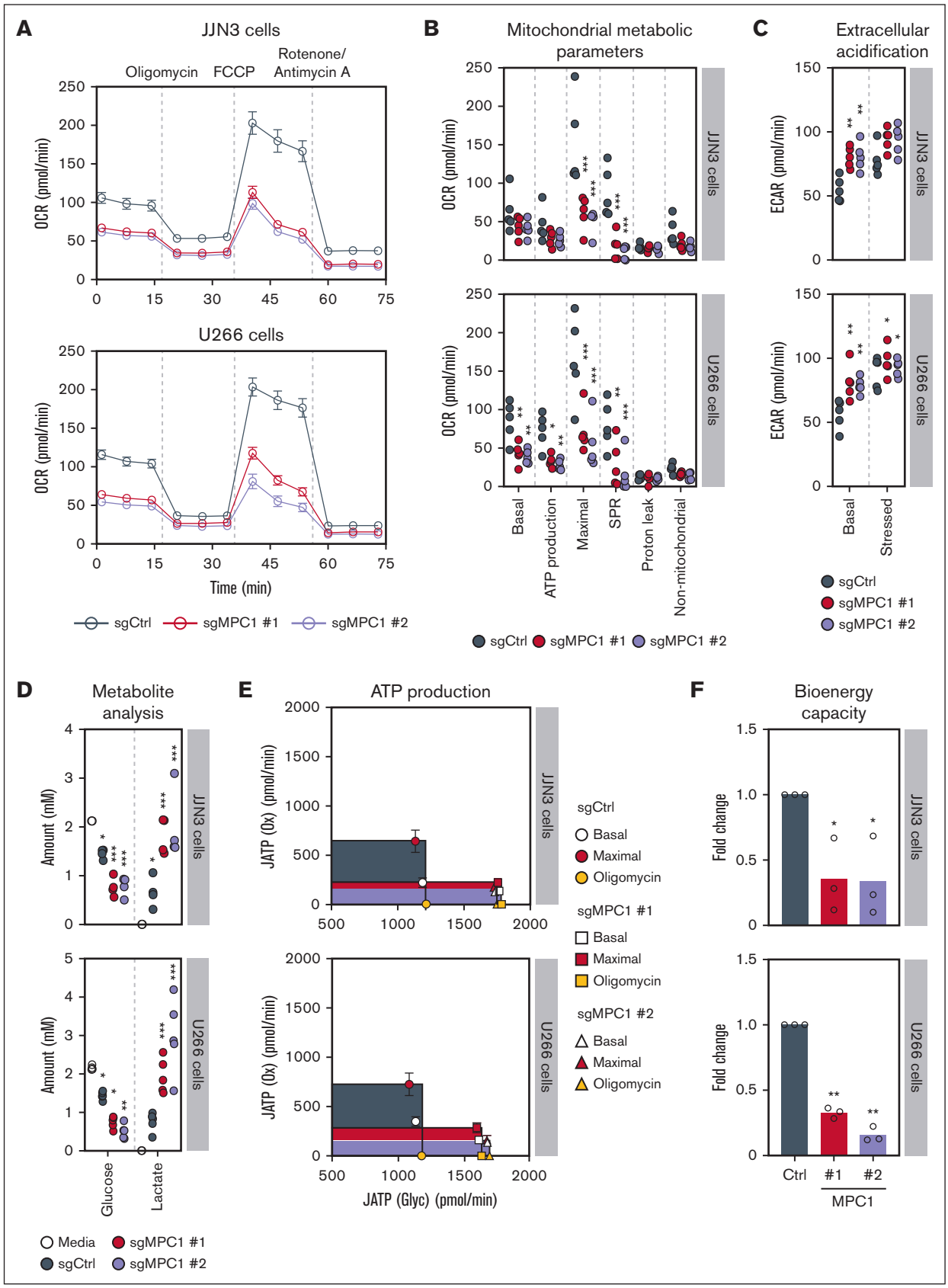

Figure 3.

To further understand the role of MPC inhibition on glutamine TCA cycle anaplerosis, we performed ^{13}C-labeled glutamine tracer loading of TCA metabolites in U266 cells (supplemental Figure 4G).[49] Across all treatments, we observed high and equal levels of ^{13}C-labeled glutamine, indicating uniform tracer loading (>95%). Notably, we noticed significantly increased M + 5 or M + 4 TCA cycle intermediates upon MPC inhibition, in the presence or absence of BTZ, beginning at the α-KG entry point throughout the most distal TCA cycle metabolite measured, malate (supplemental Figure 4H). These data are indicative of greater glutamine anaplerosis upon inhibition of the MPC complex, as previously described.[47] Of note, TCA cycle metabolite pool sizes were significantly decreased, indicating that anaplerotic compensation was incomplete (supplemental Figure 4I). Notably, UK-5099–induced TCA cycle pool size decreases were greatest upstream of α-KG, as exemplified by citrate, in comparison with no decrease in the α-KG pool size, further denoting glutamine anaplerosis (supplemental Figure 4I). These data demonstrate that MM cells rely on glutamine influx into the TCA cycle to compensate for the loss of mitochondrial pyruvate import.

Previous work has shown that glutamine starvation inhibits the proteolytic activity of the ubiquitin proteasome in monocytes.[50] Thus, we wondered whether the underlining metabolic rewiring caused by the lack of mitochondrial pyruvate import may indirectly impair proteasomal activity in MM cells. As predicted, we observed a significant reduction in the 20S proteasomal activity of *MPC1*-knockout vs control U266 cells (Figure 4E), which is further exacerbated by the addition of BTZ. In line with these findings, we noted that the pharmacological inhibition of the MPC complex in combination with a suboptimal dose of BTZ (4 nM) further inhibits the proteolytic activity of U266 cells compared with monotherapy (Figure 4F). Strikingly, glutamine starvation alone impairs the proteolytic activity of U266 cells (Figure 4G), confirming the interplay between glutamine and ubiquitin-dependent proteolysis.[50] Furthermore, inhibition with with CB-839 of the glutaminase glutaminase that converts glutamine into glutamate (5 μM) enhances BTZ-induced MM death in vitro (Figure 4H),[13,51] alike what we observed when we targeted the MPC complex. Altogether, these data suggest that glutamine anaplerosis observed upon inhibition of the MPC complex in MM cells may mimic glutamine starvation, thereby impairing proteasomal activity and potentiating BTZ-induced cell death.

Pyruvate metabolism has prognostic potential for the survival of patients with MM

To investigate the clinical relevance of our findings, we used 2 distinct cohorts of patients with MM (GSE6477 and GSE2113) among whom transcriptomic analysis was performed in early and late stages of the disease (supplemental Figure 5A), and we focused our attention on the expression of genes involved in pyruvate metabolism (supplemental Figure 5B). Interestingly, several regulators of pyruvate metabolism, including *MPC1*, *LDHB*, and *DLAT*, were differently expressed between MGUS and naive or relapsed MM in the first cohort of patients (GSE6477; Figure 5A). We made similar observations between MGUS, MM, and plasma cell leukemia, a more aggressive stage of MM, in an independent cohort of patients (GSE2113; Figure 5B), suggestive of a transcriptionally driven metabolic rewiring of MM cells during the course of this disease.

We extended our analysis to the MMRF CoMMpass database (n = 921), in which the majority of patients had been treated with a proteasome inhibitor–based regimen, and investigated the prognostic potential of pyruvate metabolism on patient outcome. Strikingly, the high expression of our pyruvate metabolic signature correlated with a significantly poorer overall survival of patients with MM (median, $P < .0001$; Figure 5C). Moreover, high expressors of this pyruvate metabolic signature display a significantly poorer progression-free survival (median, $P < .0001$; Figure 5C).

To validate our clinical analysis, we tested the efficacy of UK-5099 in potentiating BTZ response in samples from patients with MM. Strikingly, cotreatment with UK-5099 and BTZ of 4 different human MM samples significantly impaired the viability of MM cells (Figure 5D). Altogether, these data highlight the importance of pyruvate metabolism in the pathobiology of MM and its response to proteasome inhibitors (Figure 5E), thereby delineating it as a potential prognostic biomarker and therapeutic target for the treatment of MM.

Discussion

Over the past 2 decades, proteasome inhibitors have revolutionized the treatment of patients with MM by exploiting the heightened dependency of MM cells on the protein QC pathway as a therapeutic target.[2] Problematically, MM cells can acquire resistance to proteasome inhibitors through both genetic and nongenetic mechanisms,[52] highlighting our knowledge gap on the biological pathways that influence the clinical effectiveness of this class of drugs. Previous studies have endeavored to map the genetic dependencies of MM cells in response to proteasome inhibitors using RNA interference technology.[4,6,7] Here, we developed a high-throughput approach that is based on CRISPR technology to systematically interrogate the factors that influence the response of MM cells to BTZ in vitro, allowing the identification of a restricted number of novel modulators of proteasome inhibitors.[5]

As expected, our pipeline showed that targeting subunits of the 19S proteasome, including PSMC5, PSMD5, and PSMD7, protect MM cells from proteasome inhibitors, as previously described.[6,53] In turn, loss of a functional 20S proteasome further sensitizes

Figure 3. The MPC complex is required for bioenergetic capacity of MM cells. (A) OCR monitored by the Seahorse XF96 extracellular flux analyzer in JJN3 and U266 cells (n = 5). (B) Analysis of the different mitochondrial metabolic parameters obtained from the OCR in panel A. Significance was determined using two-way ANOVA followed by a Dunnett test. *$P \leq .05$; **$P \leq .005$; ***$P < .0001$. (C) Quantification of basal ECAR and stressed ECAR in JJN3 and U266 cells (n = 5). Significance was determined using two-way ANOVA followed by a Dunnett test. *$P \leq .05$; **$P \leq .005$. (D) Media metabolite analysis of JJN3 (n = 4) and U266 cells (n = 5), with a focus on extracellular glucose and lactate. Significance was determined using two-way ANOVA followed by a Dunnett test. *$P \leq .05$; **$P \leq .005$; ***$P < .0001$. (E) The metabolic capacity and flexibility of cells were represented by plotting the basal, oligomycin-treated, and maximal rates of ATP production from glycolysis (J_{ATP} gly) and oxidative phosphorylation (J_{ATP} ox), upon MPC1 knockout in both JJN3 and U266 cells (n = 5). (F) Fold change in the bioenergetic capacity and of cells described in panel A (n = 5). Significance was determined using two-way ANOVA followed by a Dunnett test. *$P \leq .05$. OCR, oxygen consumption rate.

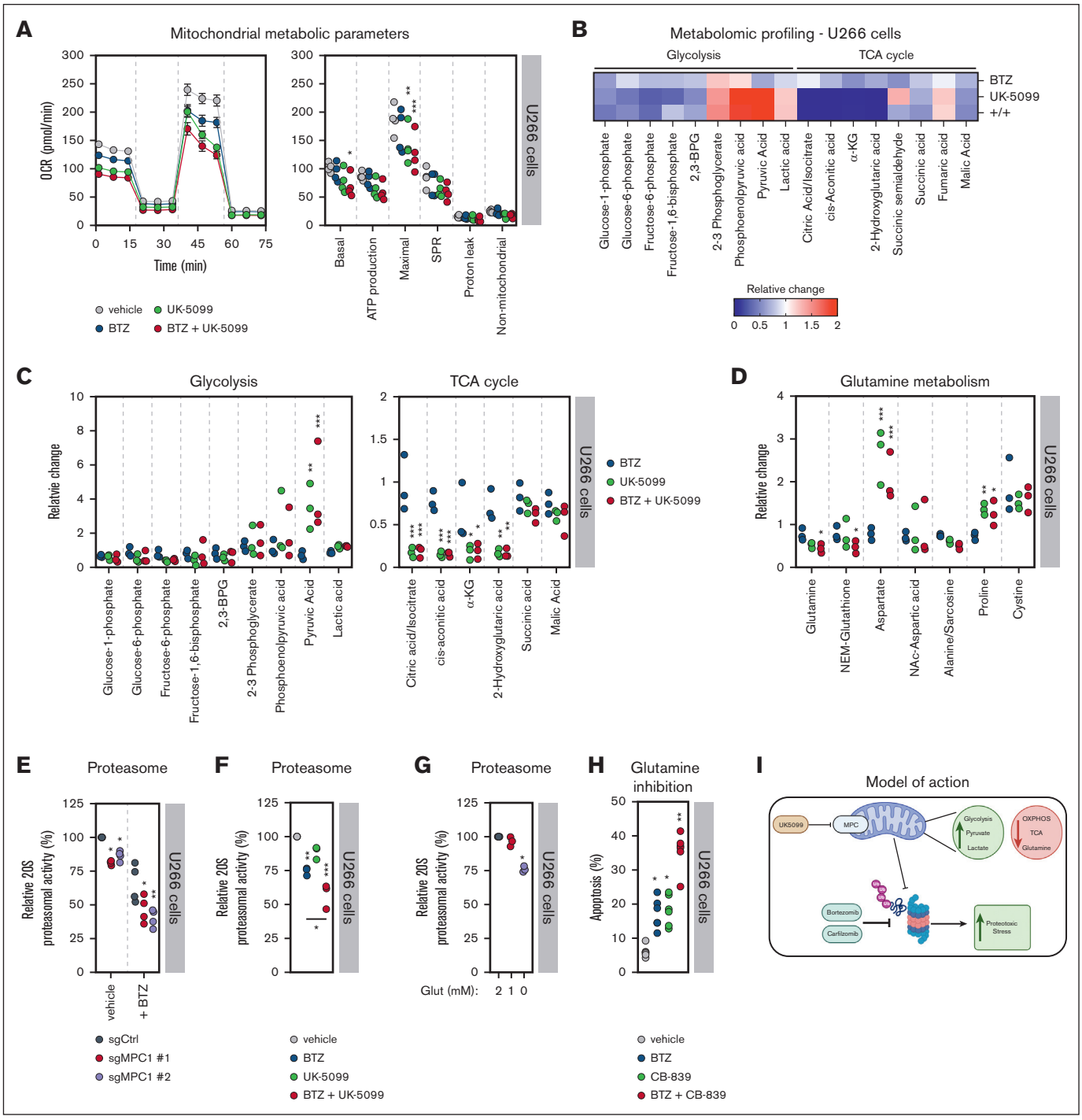

Figure 4. Lack of mitochondrial pyruvate import alters glutamine metabolism and BTZ-driven proteasomal inhibition in MM cells. (A) OCR plot and metabolic parameters of U266 cells treated with the indicated drugs: BTZ (3 nM), UK-5099 (10 μM), or the combination. Significance was determined using two-way ANOVA followed by a Dunnett test. *$P \leq .05$; **$P \leq .005$; ***$P < .0001$. (B) LC-MS results of glycolysis and the TCA cycle of monotherapies and combinatorial therapies relative to vehicle control U266 cells (n = 3). U266 cells were treated with BTZ (3 nM), UK-5099 (10 μM), or a combination for 24 hours. (C) Representation of data shown in panel B. Significance was determined using two-way ANOVA followed by a Dunnett test. *$P \leq .05$; **$P \leq .005$; ***$P < .0001$. (D) Representation of LC-MS data presented in panel B with a focus on glutamine metabolism and its associated nonessential amino acids. Significance was determined using two-way ANOVA followed by a Dunnett test. *$P \leq .05$; **$P \leq .005$; ***$P < .0001$. (E) Chymotrypsin-like proteasome activity was monitored in control (sgCtrl) or MPC1-knockout (sgMPC1 #1 and #2) U266 cells in the presence or absence (vehicle) of BTZ (3 nM) (n = 3). Significance was determined using two-way ANOVA followed by a Dunnett test. *$P \leq .05$; **$P \leq .005$. (F) Similar to panel E, except that U266 cells were treated with either vehicle, BTZ (3 nM), UK-5099 (10 μM), or the combination (n = 3). Significance was determined by two-way ANOVA followed by a Dunnett test. *$P \leq .05$; **$P \leq .005$; ***$P < .0001$. (G) Similar to panel E, except that glutamine was depleted from the media of U266 cells (basal concentration: 2 mM) (n = 3). Significance was determined using two-way ANOVA followed by a Dunnett test; * $P < .0001$. (H) U266 cells were treated with BTZ (3 nM) and the glutaminase inhibitor CB-839 (5 μM) for 48 hours, followed by an assessment of cell viability via PI. Significance was determined using two-way ANOVA followed by a Dunnett test. *$P \leq .005$; **$P \leq .0001$. (I) Schematic representing link between the MPC complex, the metabolic rewiring induced its inhibition, and the proteasomal capacity of MM cells.

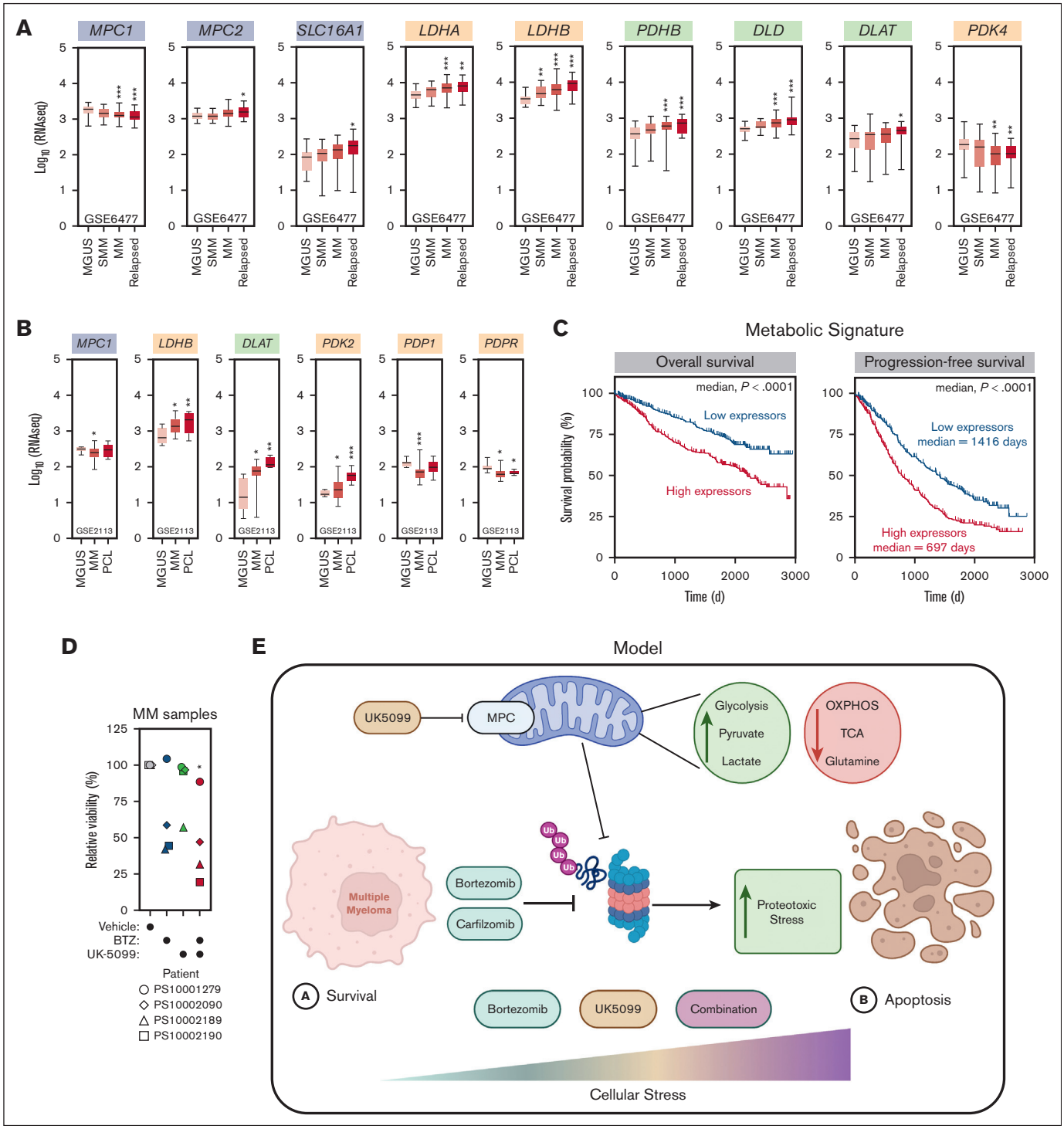

Figure 5. Pyruvate metabolism has prognostic potential for patients with MM. (A) Expression profiling of genes related to pyruvate metabolism at different stages of MM: MGUS (n = 22), SMM (n = 24), MM (n = 73), and relapsed MM (n = 28). Significance was determined using two-way ANOVA followed by a Dunnett test. *$P \leq .05$; **$P \leq .005$; ***$P < .0001$. (B) Expression profiling of genes related to pyruvate metabolism at different stages of MM in the GSE2113 data set: MGUS (n = 6), MM (n = 20), and PCL (n = 5). Significance was determined using two-way ANOVA followed by a Dunnett test. *$P \leq .05$; **$P \leq .005$; ***$P < .0001$. (C) The x-axis represents the survival time (days), and the y-axis represents survival probability (left) and progression-free survival (right). The survival analysis of the overall survival and progression-free survival in pyruvate metabolism^{high} and pyruvate metabolism^{low} groups of 772 patients with MM in the MMRF database. Significance was determined using Gehan-Breslow-Wilcoxon test. (D) Samples from patients with MM were treated with BTZ (2.5-5 nM), UK-5099 (5 μM), or the combination for 24 hours (n = 4). CD38-PE and CD45-APC-Cy7 were used to gate on MM cells. An assessment of cell viability was performed using annexin-V/DAPI staining. Significance was determined by two-way ANOVA followed by a Dunnett test. *$P \leq .05$. (E) Schematic representing our recent findings on the contribution of the MPC complex in the response to proteasome inhibitors and function in MM cells. OXPHOS, oxidative phosphorylation; PCL, plasma cell leukemia; SMM, smoldering MM.

MM cells to BTZ in vitro, highlighting the opposing effects of the catalytic core and the regulatory subunits of the proteasome on the response to proteasome inhibitors.[6] Our approach identified additional MM-specific dependencies, including the transcriptional factor IRF4.[33] Previous work has described the addiction of MM cells toward this transcription factor and its associated regulatory network,[54] and analysis of BTZ resistance in blood cancer lines correlated with an increased expression of IRF4,[55] in line with our findings that loss of IRF4 sensitizes MM cells to proteasome inhibitors. Of interest to this study, we noticed that a series of genes linked to mitochondrial metabolism potentiates the efficacy of BTZ in at least MM cell line, including the nicotinamide adenine dinucleotide hydrogen dehydrogenase NDUFA7 alongside the pyruvate kinase pyruvate kinase muscle isozyme, both subunits (PDHA and PDHB) of the pyruvate dehydrogenase complex, and both subunits of the MPC complex, highlighting the critical contribution of mitochondrial metabolism in the response to proteasome inhibitors.[12]

After decades of research on mitochondrial pyruvate metabolism, the recent identification of the molecular components that form the MPC (eg, MPC1 and MPC2) revolutionized this research area. In-depth analysis of this complex has suggested that MPC1 is critical to the stability of MPC2 protein[39], an observation that we confirmed in our MPC1-knockout MM cell lines. Rather than identifying the sole contribution of MPC1 in MM cells, our study characterized the global contribution of the MPC complex in this subset of hematological malignancies. Not surprisingly, our findings are in line with previous reports, which described the central role of the MPC complex in the bioenergetic capacities of both healthy and cancerous cells.[56-59] More importantly, our study highlights the importance of glutaminolysis as an alternative energy source in response to impaired mitochondrial pyruvate transport, which was initially observed in glioma cells.[47] Glutamine is considered the most abundant amino acid in the blood[60] and could therefore be a critical energy supply for the maintenance of MM cells and their survival in response to proteasome inhibitors.[13,51,61,62]

Proteasome inhibition has been shown to act through multiple mechanisms to induce cell death, including the activation of the unfolded protein response, the inhibition of the nuclear factor κB pathway and the induction of apoptosis through JNK and p53.[63] However, it remains largely unexplored how proteasome inhibitors may influence the metabolism of MM cells and indirectly compromise their survival. Proteasome activity has been shown to regulate T-lymphocyte metabolism and cell fate,[64] whereas proteasome inhibitors, through the modulation of c-myc levels, have been demonstrated to affect glutamine metabolism in renal cell carcinoma.[48] In turn, work in monocytes has pointed toward a direct link between glutaminolysis and proteasome activity.[50] Our data suggest that the efficacy of proteasome inhibitors may be linked to the bioenergetic state of MM cells and their ability to induce a metabolic rewiring toward glutamine metabolism.

Altogether, our study defines mitochondrial pyruvate transport as a novel modulator of proteasome inhibitors in MM cells, thereby providing a rational for the targeting of this metabolic pathway in the treatment of this hematological malignancy. Analysis of proteasome inhibitor–resistant MM has highlighted the metabolic switch that occurs in these cells: high glycolytic activity and increased serine metabolism have been linked to BTZ resistance in MM cells.[9,10] A metabolic switch toward higher mitochondrial metabolism, protein folding, and sphingomyelin synthesis was also observed in BTZ- and CFZ-resistant MM cells,[12] suggesting a central role for metabolic rewiring in the adaptation of MM cells to proteasome inhibitors. Importantly, our findings delineate potential resistance mechanisms, including metabolic rewiring toward glutaminolysis, as potential compensatory pathways to consider in the therapeutic evaluation of MPC inhibitors.

Acknowledgments

The authors are grateful to Josie Ursini Siegel, Melissa Bates, and Michael Tomasson for providing insightful suggestions on this project and useful reagents. The authors thank Adam J. Rauckhorst for his assistance with the ^{13}C-L-glutamine tracing experiments.

The authors thank Daina Avizonis, Mariana De Sa Tavares Russo, and the metabolomics core facility at McGill University, which is supported by the Canada Foundation for Innovation, the Dr. John R. and Clara M. Fraser Memorial Trust, the Terry Fox Foundation (TFF Oncometabolism team grant; TFF-242122); and McGill University. S.F. is a recipient of a Cole Foundation (Canada) doctoral scholarship. I.T. is supported by Fonds de Recherche du Québec - Santé Senior Investigator award and his laboratory is supported by Terry Fox Foundation Oncometabolism team grant TFF-242122. Work in the MS laboratory is supported by a National Institutes of Health/National Cancer Institute R01 grant (1R01CA208328-01A1) and a Leukemia and Lymphoma Society TRP award (#0000067358). L.H. is supported by Fonds de Recherche du Québec - Santé Junior 1 Investigator award and her laboratory is supported by a transition grant from the Cole Foundation (Canada), an internal operating fund from the Hôpital Maisonneuve-Rosemont Foundation, and a CIHR project grant (#201903). A.O. is the Canada Research Chair Tier 2 in genome stability and hematological malignancies. Work performed in the laboratory of A.O. was supported by a CIHR project grant (#376245), a transition grant from the Cole Foundation (Canada), an internal operating fund from the Sir Mortimer B. Davis Foundation of the Jewish General Hospital, and a start-up fund from the Department of Radiation Oncology of Emory School of Medicine.

Authorship

Contribution: S.F. designed and completed all the experiments presented in the manuscript, analyzed all data, and helped in writing the manuscript; R.N., under the supervision of M. Shanmugam, designed and completed all the experiments on samples derived from patients with MM, analyzed the data, and helped in writing the manuscript; R.A.M., under the supervision of E.B.T., designed and completed all the ^{13}C-L-glutamine tracing experiments, analyzed the data, and helped in writing the manuscript; Z.K., A.C., Z.A., and J.H., under the supervision of S.F., helped in the generation of reagents necessary for the experiments presented in the manuscript; C.S.-L., under the supervision of J.S.-P., and D.P., under the supervision of I.T., helped in the optimization of the Seahorse assay; M. Sebag helped in the analysis of patient data; L.H. helped in the analysis of the metabolomic profiling via LC-MS; A.H.K. helped in writing the manuscript; and A.O.

conceived the study, designed the research, provided supervision, and wrote the manuscript with input from all the other authors.

Conflict-of-interest disclosure: The authors declare no competing financial interests.

ORCID profiles: R.N., 0000-0002-6898-3424; J.H., 0000-0003-3439-3298; E.B.T., 0000-0003-4549-6567.

Correspondence: Alexandre Orthwein, Department of Radiation Oncology, Winship Cancer Center Emory University Atlanta, Atlanta, GA 30322; email: alexandre.orthwein@emory.edu.

References

1. Padala SA, Barsouk A, Barsouk A, et al. Epidemiology, staging, and management of multiple myeloma. *Med Sci (Basel)*. 2021;9(1):3.
2. Gulla A, Anderson KC. Multiple myeloma: the (r)evolution of current therapy and a glance into future. *Haematologica*. 2020;105(10):2358-2367.
3. Bazarbachi AH, Al Hamed R, Malard F, Harousseau JL, Mohty M. Relapsed refractory multiple myeloma: a comprehensive overview. *Leukemia*. 2019;33(10):2343-2357.
4. Zhu YX, Tiedemann R, Shi CX, et al. RNAi screen of the druggable genome identifies modulators of proteasome inhibitor sensitivity in myeloma including CDK5. *Blood*. 2011;117(14):3847-3857.
5. Shi CX, Kortum KM, Zhu YX, et al. CRISPR genome-wide screening identifies dependence on the proteasome subunit PSMC6 for bortezomib sensitivity in multiple myeloma. *Mol Cancer Ther*. 2017;16(12):2862-2870.
6. Acosta-Alvear D, Cho MY, Wild T, et al. Paradoxical resistance of multiple myeloma to proteasome inhibitors by decreased levels of 19S proteasomal subunits. *Elife*. 2015;4:e08153.
7. Chen S, Blank JL, Peters T, et al. Genome-wide siRNA screen for modulators of cell death induced by proteasome inhibitor bortezomib. *Cancer Res*. 2010;70(11):4318-4326.
8. Tiedemann RE, Zhu YX, Schmidt J, et al. Identification of molecular vulnerabilities in human multiple myeloma cells by RNA interference lethality screening of the druggable genome. *Cancer Res*. 2012;72(3):757-768.
9. Maiso P, Huynh D, Moschetta M, et al. Metabolic signature identifies novel targets for drug resistance in multiple myeloma. *Cancer Res*. 2015;75(10):2071-2082.
10. Zaal EA, Wu W, Jansen G, Zweegman S, Cloos J, Berkers CR. Bortezomib resistance in multiple myeloma is associated with increased serine synthesis. *Cancer Metab*. 2017;5:7.
11. Soriano GP, Besse L, Li N, et al. Proteasome inhibitor-adapted myeloma cells are largely independent from proteasome activity and show complex proteomic changes, in particular in redox and energy metabolism. *Leukemia*. 2016;30(11):2198-2207.
12. Besse L, Besse A, Mendez-Lopez M, et al. A metabolic switch in proteasome inhibitor-resistant multiple myeloma ensures higher mitochondrial metabolism, protein folding and sphingomyelin synthesis. *Haematologica*. 2019;104(9):e415-e419.
13. Thompson RM, Dytfeld D, Reyes L, et al. Glutaminase inhibitor CB-839 synergizes with carfilzomib in resistant multiple myeloma cells. *Oncotarget*. 2017;8(22):35863-35876.
14. Riz I, Hawley TS, Marsal JW, Hawley RG. Noncanonical SQSTM1/p62-Nrf2 pathway activation mediates proteasome inhibitor resistance in multiple myeloma cells via redox, metabolic and translational reprogramming. *Oncotarget*. 2016;7(41):66360-66385.
15. Ortiz-Ruiz A, Ruiz-Heredia Y, Morales ML, et al. Myc-related mitochondrial activity as a novel target for multiple myeloma. *Cancers (Basel)*. 2021;13(7):1662.
16. Findlay S, Heath J, Luo VM, et al. SHLD2/FAM35A co-operates with REV7 to coordinate DNA double-strand break repair pathway choice. *EMBO J*. 2018;37(18):e100158.
17. Li B, Tang J, Yang Q, et al. NOREVA: normalization and evaluation of MS-based metabolomics data. *Nucleic Acids Res*. 2017;45(W1):W162-W170.
18. Yuan J, Bennett BD, Rabinowitz JD. Kinetic flux profiling for quantitation of cellular metabolic fluxes. *Nat Protoc*. 2008;3(8):1328-1340.
19. Mookerjee SA, Gerencser AA, Nicholls DG, Brand MD. Quantifying intracellular rates of glycolytic and oxidative ATP production and consumption using extracellular flux measurements. *J Biol Chem*. 2017;292(17):7189-7207.
20. Andrzejewski S, Klimcakova E, Johnson RM, et al. PGC-1alpha promotes breast cancer metastasis and confers bioenergetic flexibility against metabolic drugs. *Cell Metab*. 2017;26(5):778-787.e5.
21. Bajpai R, Sharma A, Achreja A, et al. Electron transport chain activity is a predictor and target for venetoclax sensitivity in multiple myeloma. *Nat Commun*. 2020;11(1):1228.
22. Sharma A, Nair R, Achreja A, et al. Therapeutic implications of mitochondrial stress-induced proteasome inhibitor resistance in multiple myeloma. *Sci Adv*. 2022;8(39):eabq5575.
23. Fernando RC, de Carvalho F, Mazzotti DR, et al. Multiple myeloma cell lines and primary tumors proteoma: protein biosynthesis and immune system as potential therapeutic targets. *Genes Cancer*. 2015;6(11-12):462-471.
24. Hanamura I. Gain/amplification of chromosome arm 1q21 in multiple myeloma. *Cancers (Basel)*. 2021;13(2):256.
25. Hart T, Chandrashekhar M, Aregger M, et al. High-resolution CRISPR screens reveal fitness genes and genotype-specific cancer liabilities. *Cell*. 2015;163(6):1515-1526.

26. Li W, Xu H, Xiao T, et al. MAGeCK enables robust identification of essential genes from genome-scale CRISPR/Cas9 knockout screens. *Genome Biol*. 2014;15(12):554.
27. Yarde DN, Oliveira V, Mathews L, et al. Targeting the Fanconi anemia/BRCA pathway circumvents drug resistance in multiple myeloma. *Cancer Res*. 2009;69(24):9367-9375.
28. Murakawa Y, Sonoda E, Barber LJ, et al. Inhibitors of the proteasome suppress homologous DNA recombination in mammalian cells. *Cancer Res*. 2007; 67(18):8536-8543.
29. Jacquemont C, Taniguchi T. Proteasome function is required for DNA damage response and fanconi anemia pathway activation. *Cancer Res*. 2007; 67(15):7395-7405.
30. Maes A, Menu E, Veirman KD, Maes K, Vand Erkerken K, De Bruyne E. The therapeutic potential of cell cycle targeting in multiple myeloma. *Oncotarget*. 2017;8(52):90501-90520.
31. Zismanov V, Attar-Schneider O, Lishner M, Heffez Aizenfeld R, Tartakover Matalon S, Drucker L. Multiple myeloma proteostasis can be targeted via translation initiation factor eIF4E. *Int J Oncol*. 2015;46(2):860-870.
32. Mancino M, Grosso S, Terragna C, Borsi E, Cavo M, Biffo S. Cap dependent translation contributes to resistance of myeloma cells to bortezomib. *Translation (Austin)*. 2013;1(2):e27245.
33. Agnarelli A, Chevassut T, Mancini EJ. IRF4 in multiple myeloma-biology, disease and therapeutic target. *Leuk Res*. 2018;72:52-58.
34. Settino M, Cannataro M. Using MMRFBiolinks R-package for discovering prognostic markers in multiple myeloma. *Methods Mol Biol*. 2022;2401: 289-314.
35. Bricker DK, Taylor EB, Schell JC, et al. A mitochondrial pyruvate carrier required for pyruvate uptake in yeast, Drosophila, and humans. *Science*. 2012; 337(6090):96-100.
36. Herzig S, Raemy E, Montessuit S, et al. Identification and functional expression of the mitochondrial pyruvate carrier. *Science*. 2012;337(6090):93-96.
37. Girish V, Sheltzer JM. A CRISPR competition assay to identify cancer genetic dependencies. *Bio Protoc*. 2020;10(14):e3682.
38. Ruiz-Iglesias A, Manes S. The importance of mitochondrial pyruvate carrier in cancer cell metabolism and tumorigenesis. *Cancers (Basel)*. 2021;13(7): 1488.
39. Oonthonpan L, Rauckhorst AJ, Gray LR, Boutron AC, Taylor EB. Two human patient mitochondrial pyruvate carrier mutations reveal distinct molecular mechanisms of dysfunction. *JCI Insight*. 2019;5(13):e126132.
40. Tavoulari S, Schirris TJ, Mavridou V, et al. Key features of inhibitor binding to the human mitochondrial pyruvate carrier hetero-dimer. *Mol Metab*. 2022; 60:101469.
41. Plesca D, Mazumder S, Almasan A. DNA damage response and apoptosis. *Methods Enzymol*. 2008;446:107-122.
42. Zangari J, Petrelli F, Maillot B, Martinou JC. The multifaceted pyruvate metabolism: role of the mitochondrial pyruvate carrier. *Biomolecules*. 2020;10(7): 1068.
43. Talior I, Yarkoni M, Bashan N, Eldar-Finkelman H. Increased glucose uptake promotes oxidative stress and PKC-delta activation in adipocytes of obese, insulin-resistant mice. *Am J Physiol Endocrinol Metab*. 2003;285(2):E295-302.
44. Zhou J, Deo BK, Hosoya K, et al. Increased JNK phosphorylation and oxidative stress in response to increased glucose flux through increased GLUT1 expression in rat retinal endothelial cells. *Invest Ophthalmol Vis Sci*. 2005;46(9):3403-3410.
45. Trnka J, Blaikie FH, Smith RAJ, Murphy MP. A mitochondria-targeted nitroxide is reduced to its hydroxylamine by ubiquinol in mitochondria. *Free Radic Biol Med*. 2008;44(7):1406-1419.
46. Wang X, Perez E, Liu R, Yan LJ, Mallet RT, Yang SH. Pyruvate protects mitochondria from oxidative stress in human neuroblastoma SK-N-SH cells. *Brain Res*. 2007;1132:1-9.
47. Yang C, Ko B, Hensley CT, et al. Glutamine oxidation maintains the TCA cycle and cell survival during impaired mitochondrial pyruvate transport. *Mol Cell*. 2014;56(3):414-424.
48. Sourbier C, Ricketts CJ, Liao PJ, et al. Proteasome inhibition disrupts the metabolism of fumarate hydratase- deficient tumors by downregulating p62 and c-Myc. *Sci Rep*. 2019;9(1):18409.
49. Tompkins SC, Sheldon RD, Rauckhorst AJ, et al. Disrupting mitochondrial pyruvate uptake directs glutamine into the TCA cycle away from glutathione synthesis and impairs hepatocellular tumorigenesis. *Cell Rep*. 2019;28(10):2608-2619.e6.
50. Zellner M, Gerner C, Munk Eliasen M, et al. Glutamine starvation of monocytes inhibits the ubiquitin-proteasome proteolytic pathway. *Biochim Biophys Acta*. 2003;1638(2):138-148.
51. Effenberger M, Bommert KS, Kunz V, et al. Glutaminase inhibition in multiple myeloma induces apoptosis via MYC degradation. *Oncotarget*. 2017; 8(49):85858-85867.
52. Gandolfi S, Laubach JP, Hideshima T, Chauhan D, Anderson KC, Richardson PG. The proteasome and proteasome inhibitors in multiple myeloma. *Cancer Metastasis Rev*. 2017;36(4):561-584.
53. Tsvetkov P, Mendillo ML, Zhao J, et al. Compromising the 19S proteasome complex protects cells from reduced flux through the proteasome. *Elife*. 2015;4:e08467.
54. Shaffer AL, Emre NCT, Lamy L, et al. IRF4 addiction in multiple myeloma. *Nature*. 2008;454(7201):226-231.

55. Perez-Galan P, Mora-Jensen H, Weniger MA, et al. Bortezomib resistance in mantle cell lymphoma is associated with plasmacytic differentiation. *Blood*. 2011;117(2):542-552.

56. Ramstead AG, Wallace JA, Lee SH, et al. Mitochondrial pyruvate carrier 1 promotes peripheral T cell homeostasis through metabolic regulation of thymic development. *Cell Rep*. 2020;30(9):2889-2899.e6.

57. Schell JC, Olson KA, Jiang L, et al. A role for the mitochondrial pyruvate carrier as a repressor of the Warburg effect and colon cancer cell growth. *Mol Cell*. 2014;56(3):400-413.

58. Koh E, Kim YK, Shin D, Kim KS. MPC1 is essential for PGC-1alpha-induced mitochondrial respiration and biogenesis. *Biochem J*. 2018;475(10):1687-1699.

59. Rossi A, Rigotto G, Valente G, et al. Defective mitochondrial pyruvate flux affects cell bioenergetics in Alzheimer's disease-related models. *Cell Rep*. 2020;30(7):2332-2348.e10.

60. Xi P, Jiang Z, Zheng C, Lin Y, Wu G. Regulation of protein metabolism by glutamine: implications for nutrition and health. *Front Biosci (Landmark Ed)*. 2011;16(2):578-597.

61. Giuliani N, Chiu M, Bolzoni M, et al. The potential of inhibiting glutamine uptake as a therapeutic target for multiple myeloma. *Expert Opin Ther Targets*. 2017;21(3):231-234.

62. Bolzoni M, Chiu M, Accardi F, et al. Dependence on glutamine uptake and glutamine addiction characterize myeloma cells: a new attractive target. *Blood*. 2016;128(5):667-679.

63. Nunes AT, Annunziata CM. Proteasome inhibitors: structure and function. *Semin Oncol*. 2017;44(6):377-380.

64. Widjaja CE, Olvera JG, Metz PJ, et al. Proteasome activity regulates CD8+ T lymphocyte metabolism and fate specification. *J Clin Invest*. 2017;127(10):3609-3623.